A Numerical Study of the Aerodynamic Characteristics of a High-Speed Train under the Effect of Crosswind and Rain

Haiqing Li[1], Mengge Yu[1, *], Qian Zhang[1] and Heng Wen[1]

Abstract: The performances of high-speed trains in the presence of coupling effects with crosswind and rain have attracted great attention in recent years. The objective of the present paper was to investigate the aerodynamic characteristics of a high-speed train under such conditions in the framework of an Eulerian-Lagrangian approach. An aerodynamic model of a high-speed train was first set up, and the side force coefficient obtained from numerical simulation was compared with that provided by wind tunnel experiments to verify the accuracy of the approach. Then, the effects of the yaw angle, the resultant wind speed, and the rainfall rate on aerodynamic coefficients were analyzed. The results indicate that the aerodynamic coefficients grow almost linearly with the rainfall rate, and increase with a decrease in the resultant wind speed. Due to the impact of raindrops on the train surface and the airflow, the pressure coefficients of windward and leeward side of the train become larger with the increase of the rainfall rate. Raindrops can accelerate the airflow and suppress the vortices detachment. Moreover, the flow velocity in regions surrounding the train increases with an increase in the rainfall rate.

Keywords: High-speed trains, Eulerian-Lagrangian, crosswinds and rains, aerodynamic coefficients, pressure coefficients, velocity distribution.

1 Introduction

With technological development, the train speed has dramatically increased over the past several decades. Improvements of the speed have deteriorated aerodynamic characteristics of high-speed trains [Schetz (2001); Yu, Jiang and Zhang (2019)], hence the aerodynamics of railway vehicles is becoming a significant issue of concern currently. In China, most of the high-speed railways are built in densely populated and economically developed areas along the eastern coast. These areas are the monsoon region, and storms and thunderstorms are common phenomena in many parts of the region. When high-speed trains run in such a severe environment, the crosswinds and rains have a great impact on the flow filed of the train, leading to increased load and creating a disturbance in the flow. Understanding coupling effects of crosswinds and rains on the performance of high-speed trains provides valuable information in operational safety.

In current years, to study aerodynamic characteristics of high-speed trains exposed to crosswinds, many experts and scholars have conducted a considerable amount of

researches through full-scale tests [Baker, Jones and Lopez-calleja (2004)], wind tunnel experiments [Giappino, Melzi and Tomasini (2018)] and numerical simulations [Hemida and Baker (2010); Yu, Liu and Liu (2016)], and found that aerodynamic forces and moments of high-speed trains in crosswinds increase sharply. The majority of investigations about the effect of rains was mainly limited to aviation applications [Bezos, Dunham and Gentry (1992); Cai, Abbasi and Arastoopour (2013); Wu, Cao and Ismail (2013); Cohan and Arastoopour (2016)] and construction industry [Choi (1992); Huang and Li (2010); Hooff, Blocken and Harten (2011)]. In these studies, two main methods were used, including a Eulerian-Eulerian model developed by Gidaspow [Gidaspow (1994)] and a Lagrangian discrete phase model (DPM) developed by Crowe et al. [Crowe and Smoot (1979)]. In these years, the effect of rainfall on the aerodynamic performance of high-speed trains has attracted great attention, and some research about aerodynamic characteristics of high-speed trains under crosswind and rain conditions has been published. Shao et al. [Shao, Wan and Chen (2011)] studied aerodynamic characteristics of a high-speed train subjected to different crosswind speeds under a train speed of 360 km/h and a rainfall rate of 60 mm/h, and found that the lift force, lateral force and the rolling moment increase sharply, which drastically deteriorates the operational safety of the train. Jing et al. [Jing and Gao (2013)] studied the effects of different rainfall rates, wind speeds and train velocities on the flow field of the train, and found that the dynamic load on train when bearing strong crosswinds and rains is a little bigger than that when bearing only strong crosswinds. Yue et al. [Yue, Zeng and Li (2016)] investigated variations in aerodynamic coefficients of high-speed trains at different yaw angles with or without rainfalls, and found a decrease of running stability of the train, compared with that under only crosswind conditions.

However, in most of the previous study, the train is reduced to a simple model ignoring too much detail structures such as windshields and bogies, which would have a large impact on the flow field of the train. Furthermore, although some preliminary studies have been conducted on aerodynamic characteristics of high-speed trains under crosswind and rain conditions when the train speed or the rainfall rate is constant, systematic investigations of the aerodynamic characteristics were not performed. Therefore, in the present study, it is the purpose to address the issues mentioned above. A high-speed train model including windshields and bogies was constructed, and the effects of yaw angles, resultant wind speeds and rainfall rates on aerodynamic coefficients were systematically investigated. In addition, surface pressure coefficient distribution and velocity distribution under different rainfall rates were studied.

2 Eulerian-Lagrangian approach

2.1 Continuous phase

To study the flow field of the train crusing in crosswinds, an approved Reynolds-averaged Navier-Stokes (RANS) turbulent model, Shear stress transport (*SST*) *k-ω* proposed by Menter [Menter (1994)], is used to slove the conservation equations of mass and momentum. The *SST k-ω* model has a capability in predicting the averaged surface pressure [Morden, Hemida and Baker (2015); Premoli, Rocchi and Schito (2016); Li, Hemida and Zhang (2018)]. The conservation equation of mass is

$$\frac{\partial \rho}{\partial t} + \nabla \cdot \left(\rho \vec{v} \right) = 0 \tag{1}$$

where ρ is the air density, $\vec{v}$ is the air velocity. And the conservation equation of momentum is

$$\frac{\partial}{\partial t} \left(\rho \vec{v} \right) + \nabla \cdot \left(\rho \vec{v} \vec{v} \right) = -\nabla p + \nabla \cdot \left(\overline{\overline{\tau}} \right) - M_{ex_i} \tag{2}$$

where p is the pressure, M_{ex_i} is the interphase momentum exchange of M_{ex} in the i direction and

$$\overline{\overline{\tau}} = \mu \left[\left(\nabla \vec{v} \right) + \nabla \vec{v}^T \right] \tag{3}$$

where μ is the air molecular turbulent viscosity.

Two transport equations are

$$\frac{\partial}{\partial t} \left(\rho k \right) + \frac{\partial}{\partial x_i} \left(\rho k u_i \right) = \frac{\partial}{\partial x_j} \left(\Gamma_k \frac{\partial k}{\partial x_j} \right) + \overline{G}_k - Y_k \tag{4}$$

$$\frac{\partial}{\partial t} \left(\rho \omega \right) + \frac{\partial}{\partial x_i} \left(\rho \omega u_i \right) = \frac{\partial}{\partial x_j} \left(\Gamma_\omega \frac{\partial \omega}{\partial x_j} \right) + G_\omega - Y_\omega + D_\omega \tag{5}$$

where $\overline{G}_k$ and G_ω are the turbulence kinetic energy and the generation of ω, while Γ_k and Γ_ω, Y_k and Y_ω are the effective diffusivity, the dissipation of k and ω, respectively. D_ω is the cross-diffusion term.

The side force coefficient C_s, the lift coefficient C_l, the roll moment coefficient around the top of the leeward side rail C_m and the pressure coefficient C_p are adopted to estimate aerodynamic characteristics, which are defined by the expressions

$$C_s = \frac{F_s}{0.5 \rho V^2 S}, C_l = \frac{F_l}{0.5 \rho V^2 S}, C_m = \frac{M_m}{0.5 \rho V^2 S l}, C_p = \frac{P}{0.5 \rho V^2} \tag{6}$$

where F_s, F_l and M_m denote the side, lift force and roll moment around the top of the leeward side rail, respectively. ρ is the air density, V is the resultant wind velocity, P is the relative pressure, S is the train reference area, S=11.12 m^2, and l is the feature height, which is 3.7 m here.

2.2 Discrete phase

The amount of raindrops per unit volume of air is on the order of about one thousandth, far below 10 percent. In order to modeling rainfalls, a Lagrangian DPM was adopted for tracking the raindrops. The force balance equation of the raindrops in the DPM is

$$\frac{du_p}{dt} = F_D \left(u - u_p \right) + \frac{g_x \left(\rho_p - \rho \right)}{\rho_p} \tag{7}$$

where u, u_p and ρ_p are the air velocity, the raindrop velocity and the raindrop density respectively, g_x is the gravity acceleration of g in the x direction and the $F_D(u-u_p)$ is the drag force per unit raindrop mass. F_D is defined as

$$F_D = \frac{3C_D(u-u_p)}{4d_p} \tag{8}$$

where d_p is the raindrop diameter. The spherical drag law was adopted to measure the drag coefficient C_D [Morsi and Alexander (1972)].

$$C_D = a_1 + \frac{a_2}{Re} + \frac{a_3}{Re^2} \tag{9}$$

where constants a_1, a_2 and a_3 are relative to the Reynolds number Re.

In order to develop numerical model of the effect of rain on aerodynamic characteristics of high-speed trains, the phenomenon of naturally occurring precipitation needs to be understood. A parameter quantity generally used to describe rain is the rainfall rate I, which is in mm/h and is a water depth at ground level per hour. Equivalently, as a function of I, W in mm^3/m^3 was chosen to categorize different rainfall rates, which is the amount of raindrops per unit volume of air [Best (1950)] and is expressed as

$$W = CI^r \tag{10}$$

where the values of constants C and r are 67 and 0.846, respectively.

It is essential to set up raindrop size distribution under different rain rates. The size of raindrops is nonuniform, many researchers have summarized various formulas. To simplify calculations, the raindrop diameter which accounts for the most volume of water in the air, was chosen as the predominant drop diameter D by Best [Best (1950)]

$$D = a\left(\frac{n-1}{n}\right)^{\frac{1}{n}} \tag{11}$$

where

$$a = AI^p \tag{12}$$

and the constants A, p and n are 1.3, 0.232 and 2.25, respectively.

In addition, raindrops will reach a constant velocity before hitting the train surface. A formula was used to describe the terminal velocity of droplets [Best (1950)].

$$V_p = 9.58\left\{1 - \exp\left[-\left(\frac{D}{1.77}\right)^{1.147}\right]\right\} \tag{13}$$

2.3 Interphase coupling

The momentum between the continuous phase and the discrete phase exchanges due to the interphase drag forces. The discrete phase introduces the momentum source term into the momentum equation to influence the continuous phase. The interphase momentum exchange can be defined as

$$M_{ex} = \Sigma \frac{3\mu C_{D} Re_{p}}{4\rho_{p} D_{p}^{2}} \left(u - u_{p}\right) \dot{m}_{p} \Delta t \tag{14}$$

where $\dot{m}_{p}$ is the raindrop mass flow rate per unit volume.

3 Numerical model

3.1 Calculation domain and boundary conditions

The train model used in our computation was based on a CRH high-speed train. As shown in Fig. 1, the model consists of 3 cars, including a head car, a middle car and a tail car. Windshields and bogies were taken into account in this study. Fig. 2 shows the calculation domain and boundary conditions. In particular, to ensure that raindrops can touch the train adequately, the train is positioned at a distance of 850 m from the upstream boundary, and the distance from the center line of the train to the windward side boundary is 230 m.


Figure 1: Train model
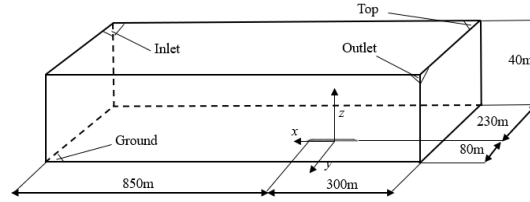
Figure 2: Domain and boundary conditions

For continuous phase, the ground and the surface of the train are set as "no-slip wall", and the top of the domain is set as a symmetrical boundary. A "velocity inlet" is used in the inlet boundary, and the outlet is set as "pressure outlet". For discrete phase, the top surface of the domain is set as "surface injection", the ground is set as "trap", the train surface is set as "wall-film", where the "stanton-rutland" collision model is adopted. The "stanton-rutland" collision model consists of four regimes, namely, stick, rebound, spread and splash, which are based on the impinging energy and wall temperature [Wu, Cao and Ismail (2013)]. And the entrance and exit are set as "escape".

Fig. 3 shows a schematic that describes the train speed v, the crosswind speed w and the wind angle α under crosswinds. In Fig. 3, u is the resultant wind speed and the wind angle is 90° in the present paper. The yaw angle β is defined as

β=arctan (w/v) \hfill (15)
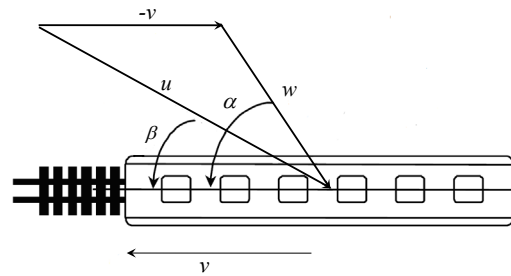
Figure 3: Schematic of the resultant wind speed

3.2 Meshing strategy and numerical method

In this study, the hexahedral-dominated grids were generated, which is shown in Fig. 4. The maximum mesh size on the train body surface is 45 mm, and on the windshields and bogies surface is 22.5 mm. To accurately obtain the flow field of the train and capture vortex shedding of the leeward side and the wake flow, 3 refinement regions were applied around the train. The mesh sizes of these 3 refinement regions are 90 mm, 180 mm, and 360 mm, respectively. In addition, the height of the first prism layer near the train is 0.01 mm to guarantee that the y+ around the train is approximately 1. And the number of prism layers is 10, the growth ratio is 1.2. A total of 27 million cells were generated. The numerical simulation was performed using the finite volume method. A pressure-based solver was used for the flow equations. And the Semi-Implicit Method for Pressure-Linked Equations (SIMPLE) algorithm was adopted for solving the coupling between pressure and velocity effects. The least squares cell-based method and the second order scheme were used to solve the gradients and the pressure equations, respectively. Moreover, a second order upwind scheme was applied to handle the momentum, turbulent kinetic energy and specific dissipation rate equations.


(a)

(b)
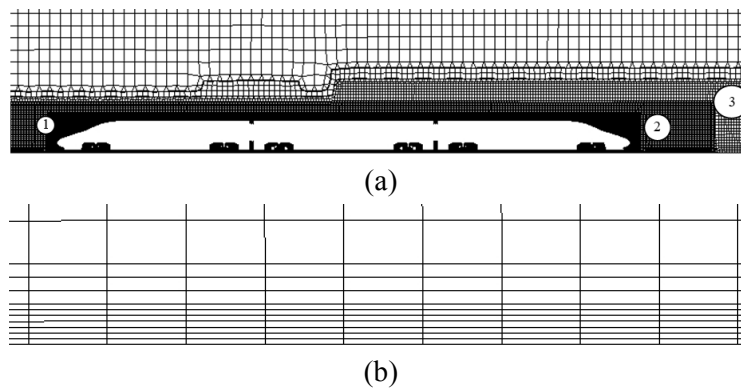
Figure 4: Mesh (a) mesh around the train (b) boundary layer

3.3 Validation

Aerodynamic force coefficients were employed to verify the reliability of the numerical simulation. A wind tunnel experiment of the 1:8 scale train model was

carried out in a wind tunnel in China, and a full description of experiment and its results was given by Zhang et al. [Zhang and Zhou (2013)]. The same train model was set up for numerical simulation in this paper so as to verify the numerical accuracy. As shown in Fig. 5, the side force coefficient of the head car was simulated and compared with the test results, for a resultant wind speed of 60 m/s, and a variety of yaw angles. It can be seen from Fig. 5 that the results obtained from the numerical simulation agree well with that from the wind tunnel test. And the difference is acceptable in engineering. Hence the turbulence model, boundary conditions, mesh resolution and so on were reliable for simulation accuracy.
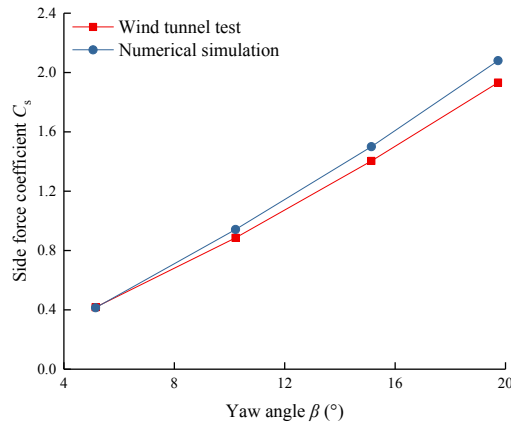
Figure 5: Comparison of the wind tunnel test and numerical simulation

4 Results and analysis

The train speed is 200 km/h, 300 km/h and 400 km/h, the crosswind velocity is 10 m/s, 20 m/s and 30 m/s, and the rainfall rate is 100 mm/h, 300 mm/h and 500 mm/h, respectively. Different combinations of vehicle speeds and wind speeds produce different yaw angles, as shown in Tab. 1.

Table 1: Different yaw angles at different train speeds and crosswind speeds

| Yaw angles (°)	Train speed (km/h)	Crosswind speed (m/s)	Yaw angles (°)	Train speed (km/h)	Crosswind speed (m/s)
5.1	400	10	15.1	400	30
6.8	300	10		200	20
	200	10	19.8	300	30
10.2					
	400	20	28.4	200	30
13.5	300	20			

4.1 Aerodynamic coefficients

Operational safety of the head car exposed to crosswind is the worst [Xi, Mao and Li (2010); Yu, Zhang and Zhang (2011); Zhang, Yang and Liang (2018)]. Therefore,

variations of the side force coefficient, the lift force coefficient and the roll moment coefficient around the leeward side rail of the head car are given in this section.

Fig. 6(a) shows variations of the side force coefficient with yaw angles in pure crosswind conditions. And Fig. 6(b) shows variations of the side force coefficient with yaw angles in crosswind and rain conditions, and the rainfall rate is 500 mm/h. It is noted that, for yaw angles of 10.2° or 19.8°, there are two different resultant wind speeds (see Tab. 1). It can be seen from Fig. 6 that, for a train exposed to crosswind, the side force coefficient is only determined by yaw angles. However, for a train exposed to crosswind and rain conditions, the resultant wind speed can also affect the side force coefficient.


| (a) | (b) |
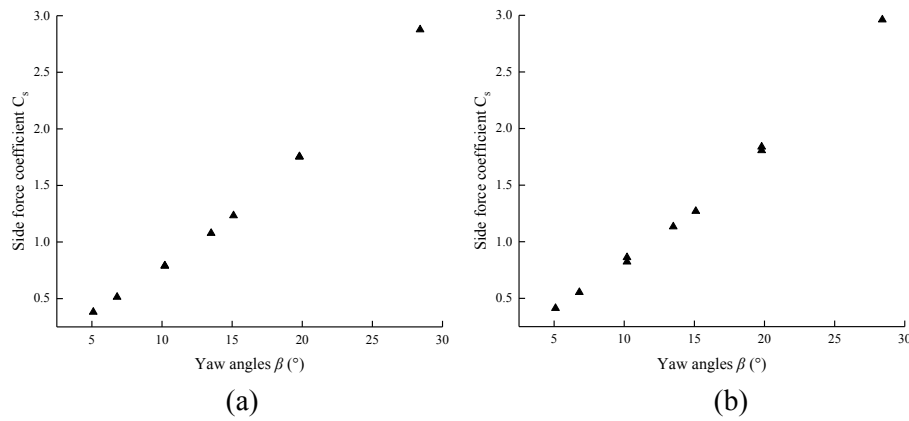
Figure 6: Variations under different rainfall rates (a) 0 mm/h (b) 500 mm/h

| (a) | (b) |
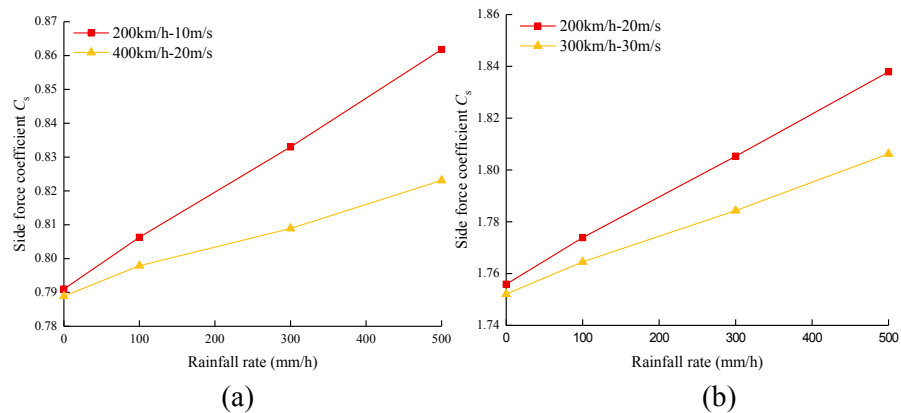
Figure 7: Variations under different yaw angles (a) β=10.2° (b) β=19.8°

Fig. 7 shows the influence of resultant wind speeds and rainfall rates on the side force coefficient for the same yaw angle. It can be observed from Fig. 7 that the effect of the resultant wind speed on the side force coefficient becomes more obvious when the rainfall rate is greater. When the yaw angle is 10.2°, for a resultant wind speed of 56.45 m/s (v=200 km/h, w=10 m/s), the side force coefficient increases by 4.7% at a rainfall rate of 500 mm/h,

compared with that for a resultant wind speed of 112.9 m/s (v=400 km/h, w=20 m/s). When the yaw angle is 19.8°, for a resultant wind speed of 59.05 m/s (v=200 km/h, w=20 m/s), the side force coefficient increases by 1.76% at a rainfall rate of 500 mm/h, compared with that for a resultant wind speed of 88.57 m/s (v=300 km/h, w=30 m/s). The side force coefficient grows almost linearly with the rainfall rate. And for the same yaw angle, the side force coefficient becomes smaller when the resultant wind speed is larger. For the lift force coefficient and the rolling moment coefficient, similar rules can be obtianed.
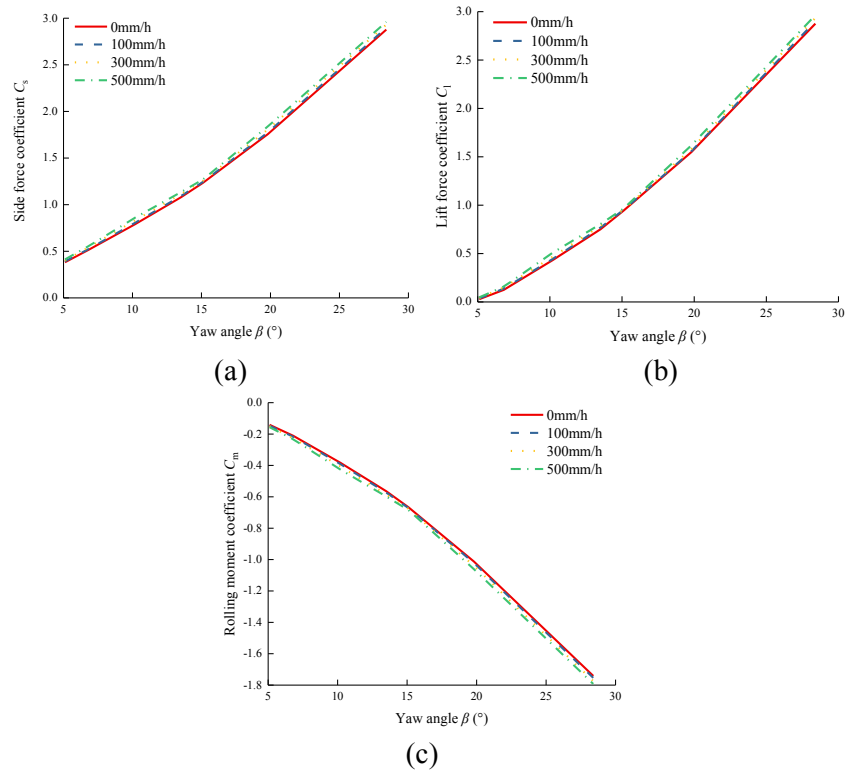

Figure 8: Variations of the aerodynamic coefficients (a) side force (b) lift force (c) rolling moment

Fig. 8 shows variations of the side force coefficient, the lift force coefficient and the roll moment coefficient with yaw angles and rainfall rates. And it's worth noting that, when the yaw angle is 10.2°, aerodynamic coefficients at the resultant wind speed of 56.45 m/s are given in Fig. 8. While for the yaw angle of 19.8°, the corresponding resultant wind speed is 59.05 m/s. It can be observed from Fig. 8(a) that the side force coefficient increases as the yaw angle increases, and is approximately quadratic with the yaw angle, which agrees well with previous studies [Tian (2010); Yu, Zhang and Zhang (2015)]. When the yaw angle is constant, it increases as the rainfall rate increases. As shown in Figs. 8(b) and (c), the lift force coefficient and the rolling moment coefficient have a similar trend.
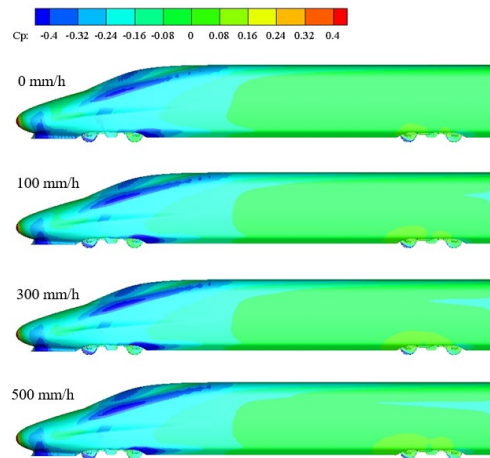
4.2 Pressure coefficient

The aerodynamic force is obtained by integrating the surface pressure coefficient, which directly influences aerodynamic forces of the train. Figs. 9 and 10 respectively show the surface pressure coefficients of the windward and leeward side, for a train speed of 200 km/h and a wind speed of 10 m/s.

It can be seen from Fig. 9 that, there is a strong positive-pressure area in the windward side of the head car, and a negative-pressure area near the top. As the rainfall rate increases from 0 mm/h to 500 mm/h, the positive pressure coefficient on the windward side of the head car increases gradually and the positive-pressure area expands.
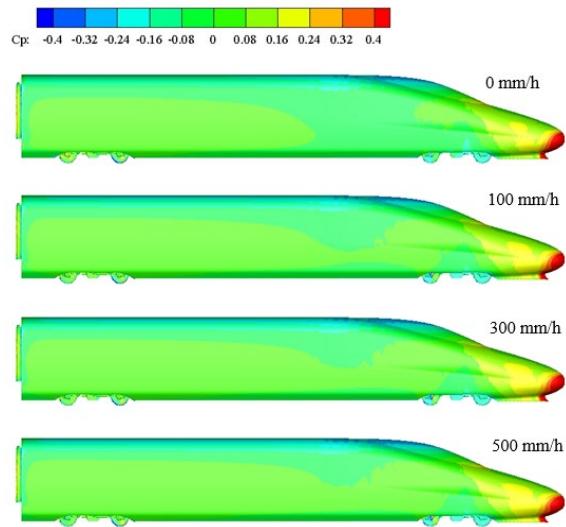
Figure 9: Pressure coefficient of windward side

It can be seen from Fig. 10 that there is a strong negative-pressure area in the leeward side of the head car, and a positive-pressure area near the second bogie. As the rainfall rate increases from 0 mm/h to 500 mm/h, the negative pressure coefficient on the leeward side of the head car increases. The negative-pressure area expands as the rainfall rate increases, especially for the streamlined zone and the area near the windshield. However, the area of the positive pressure near the second bogie also expands. It can be drawn a conclusion from Figs. 9 and 10 that the side force coefficient is positive and increases with the increase of rainfall rate.

Figure 10: Pressure coefficient of leeward side

4.3 Velocity distribution

To further analyse the flow characteristics of the head car with different rainfall rates, Fig. 11 shows the velocity distribution of the middle cross-section of the head car at x=25 m, for a train speed of 200 km/h and a crosswind speed of 10 m/s.

It can be observed from Fig. 11 that, as the rainfall rate increases from 0 mm/h to 500 mm/h, three main differences of the velocity distribution of the head car can be found in region 1, region 2 and region 3. Because the falling raindrops accelerate the airflow, the velocity of windward side increases slightly with the increase of the rainfall rate, and the area of region 1 increases as the rainfall rate increase. There are three vortices in the leeward side. And low velocity zones are formed at the center of vortices. For region 2 and 3 of the leeward side, raindrops suppress the vortices detachment so that the area of low velocity becomes smaller. And the velocity of these two regions increase with the increase of the rainfall rate.
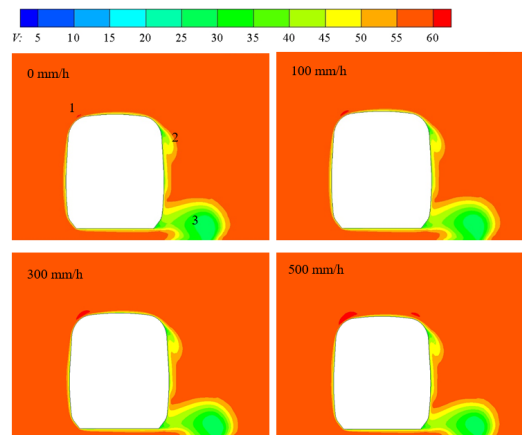
Figure 11: Velocity contours with different rainfall rates

5 Conclusions

In this paper, the aerodynamic coefficients of the head car under crosswind and rain conditions were analyzed through Eulerian-Lagrangian approach. The surface pressure coefficients distribution and velocity distribution were studied. Based on the results, several conclusions are as follows:

(1) The side force coefficient of the train exposed to crosswinds is only determined by yaw angles. However, the resultant wind speed can also affect the side force coefficient of the train under crosswind and rain conditions.

(2) The effect of the resultant wind speed on the side force coefficient becomes more obvious when the rainfall rate is greater. There is a maximum difference of 4.7% at the yaw angle of 10.2°. The side force coefficient grows almost linearly with the rainfall rate. And for the same yaw angle, the side force coefficient becomes smaller when the resultant wind speed is larger.

(3) Due to the impact of raindrops on the train surface and the airflow, the windward and leeward surface pressure coefficient become larger with the increase of the rainfall rate.

(4) Raindrops can accelerate the airflow surrounding the train and suppress the vortices detachment, so velocity surrounding the train increases with an increase in the rainfall rate.

Conflicts of Interest: The authors declare that they have no conflicts of interest to report regarding the present study.

References

Baker, C. J.; Jones, J.; Lopez-calleja, F.; Munday, J. (2004): Measurements of the crosswind forces on trains. *Journal of Wind Engineering and Industrial Aerodynamics*, vol. 92, pp. 547-563.

Best, A. C. (1950): The size distribution of raindrops. *Quarterly Journal of the Royal Meteorological Society*, vol. 76, no. 32, pp. 16-36.

Best, A. C. (1950): Empirical formulae for the terminal velocity of water drops falling through the atmosphere. *Quarterly Journal of the Royal Meteorological Society*, vol. 76, no. 329, pp. 302-311.

Bezos, G. M.; Dunham, R. E.; Gentry, G. L.; Melson, W. E. (1992): Wind tunnel aerodynamic characteristics of a transport-type airfoil in a simulated heavy rain environment. *NASA Technical*, pp. 3184.

Cai, M.; Abbasi, E.; Arastoopour, H. (2013): Analysis of the performance of a wind turbine airfoil under heavy rain condition using a multiphase CFD approach. *Industrial and Engineering Chemistry Research*, vol. 52, pp. 3266-3275.

Choi, E. C. C. (1992): Simulation of wind-driven-rain around a building. *First International Symposium on Computational Wind*, no. 52, pp. 60-65.

Cohan, A. C.; Arastoopour, H. (2016): Numerical simulation and analysis of the effect of rain and surface property on wind-turbine airfoil performance. *International Journal of Multiphase Flow*, vol. 81, pp. 46-53.

Crowe, C. T., Smoot, L. D. (1979): Multicomponent conservation equation. *Pulverized-Coal Combustion and Gasification*, Plenum Press.

Giappino, S.; Melzi, S.; Tomasini, G. (2018): High-speed freight trains for intermodal transportation: wind tunnel study on the aerodynamic coefficients of container wagons. *Journal of Wind Engineering and Industrial Aerodynamics*, vol. 175, pp. 111-119.

Gidaspow, D. (1994): *Multiphase Flow and Fluidization*. Academic Press.

Hemida, H.; Baker, C. J. (2010): Large-eddy simulation of the flow around a freight wagon subjected to a crosswind. *Computers and Fluids*, vol. 39, pp. 1944-1956.

Hooff, T. V.; Blocken, B.; Harten, M. V. (2011): 3D CFD simulations of wind flow and wind-driven rain shelter in sports stadia: influence of stadium geometry. *Building and Environment*, vol. 46, pp. 22-37.

Huang, S. H.; Li, Q. S. (2010): Numerical simulations of wind-driven rain on building envelopes based on Eulerian multiphase model. *Journal of Wind Engineering and Industrial Aerodynamics*, vol. 98, pp. 843-857.

Jing, J. E.; Gao, G. J. (2013): Simulation of the action effect of wind-driven rain on high-speed train. *Journal of Railway Science and Engineering*, vol. 10, no. 3, pp. 99-102.

Li, T.; Hemida, H.; Zhang, J. Y.; Rashidi, M.; Flynn, D. (2018): Comparisons of shear stress transport and detached eddy simulations of the flow around trains. *Journal of Fluids Engineering*, vol. 140, pp. 111108.

Menter, F. R. (1994): Two-equation eddy-viscosity turbulence models for engineering applications. *AIAA Journal*, vol. 32, no. 8, pp. 1598-1605.

Morden, J. A.; Hemida, H.; Baker, C. J. (2015): Comparison of RANS and detached eddy simulation results to wind-tunnel data for the surface pressures upon a class 43 high-speed train. *Journal of Fluids Engineering*, vol. 137, no. 4, pp. 041108.

Morsi, S. A.; Alexander, A. J. (1972): An investigation of particle trajectories in two-phase flow systems. *Journal of Fluid Mechanics*, vol. 55, no. 2, pp. 193-208.

Premoli, A.; Rocchi, D.; Schito, P.; Tomasini, G. (2016): Comparison between steady and moving railway vehicles subjected to crosswind by CFD analysis. *Journal of Wind Engineering and Industrial Aerodynamics*, vol. 156, pp. 29-40.

Schetz, J. A. (2001): Aerodynamics of high-speed trains. *Annual Review of Fluid Mechanics*, vol. 33, no. 1, pp. 371-414.

Shao, X. M.; Wan, J.; Chen, D. W.; Xiong, H. B. (2011): Aerodynamic modeling and stability analysis of a high-speed train under strong rain and crosswind conditions.

Journal of Zhejiang University-Science A (Applied Physics and Engineering), vol. 12, no. 12, pp. 964-970.

Tian, H. Q. (2010): Research progress in railway safety under strong wind condition in China. *Journal of Central South University (Science and Technology)*, vol. 41, no. 6, pp. 2435-2443.

Wu, Z. L.; Cao, Y. H.; Ismail, M. (2013): Numerical simulation of airfoil aerodynamic penalties and mechanisms in heavy rain. *International Journal of Aerospace Engineering*, pp. 590924.

Xi, Y. H.; Mao, J.; Li, M. G.; Zhang, N.; Ma, X. Y. (2010): Numerical study on the crosswind effects of high-speed train. *Journal of Beijing Jiaotong University*, vol. 34, no. 1, pp. 14-19.

Yu, M. G.; Liu, J. L.; Liu, D. W.; Chen H. M.; Zhang J. Y. (2016): Investigation of aerodynamic effects on the high-speed train exposed to longitudinal and lateral wind velocities. *Journal of Fluids and Structures*, vol. 61, pp. 347-361.

Yu, M. G.; Jiang R. C.; Zhang, Q.; Zhang, J. Y. (2019): Crosswind stability evaluation of high-speed train using different wind models, *Chinese Journal of Mechanical Engineering*, vol. 32, no. 40.

Yu, M. G.; Zhang, J. Y.; Zhang, K. Y.; Zhang, W. H. (2015): Crosswind stability analysis of a high-speed train based on fuzzy random reliability. *Institution of Mechanical Engineers, Part F: Journal of Rail and Rapid Transit*, vol. 229, no. 8, pp. 875-887.

Yu, M. G.; Zhang, J. Y.; Zhang, W. H. (2011): Wind-induced security of high-speed trains on the ground. *Journal of Southwest Jiaotong University*, vol. 46, no. 6, pp. 989-995.

Yue, Y. F.; Zeng, Q. L.; Li, Z. S.; Lu, F. A. (2016): Numerical simulating effects of rain-loaded wind on the aerodynamic characteristics and running stability of high-speed trains. *Journal of Desert Research*, vol. 36, no. 4, pp. 943-950.

Zhang, L.; Yang, M. Z.; Liang, X. F. (2018): Experimental study on the effect of wind angles on pressure distribution of train streamlined zone and train aerodynamic forces. *Journal of Wind Engineering and Industrial Aerodynamics*, vol. 174, pp. 330-343.

Zhang, Z. Z.; Zhou, D. (2013): Wind tunnel experiment on aerodynamic characteristic of streamline head of high speed train with different head shapes. *Journal of Central South University (Science and Technology)*, vol. 44, no. 6, pp. 2603-2608.